Cell Model for the Scale-up of Fluid Dynamics and Mass Transfer in Random Packed Columns Affected by Maldistribution

Jost H. Brinkmann[1*], Amelie Merkel[1], Dominik Plate[1], Prof. Dr. Marcus Grünewald[1]

[1]Ruhr-University Bochum, Laboratory of Fluid Separations, Universitätsstrasse 150, 44801 Bochum, Germany.

Email corresponding author: jost.brinkmann@ruhr-uni-bochum.de

Abstract

The characterization of fluid dynamics and mass transfer is often influenced by phase maldistribution. An existing cell model approach for fluid distribution is extended for gas distribution and mass transfer. The model differentiates wall and bulk zones, allowing a detailed evaluation of local fluid dynamics and mass transfer, which is based on a state-of-the-art literature correlation. Distribution parameters are determined experimentally. The model allows scale-up by considering the phase distribution at constant computational effort. A scale-up strategy to adapt the distribution parameters to different geometries is presented. Results for fluid dynamics and liquid distribution are in good agreement with experimental data of columns with diameters of 0.288, 0.5 and 0.6 m. Mass transfer is in good qualitative agreement with own experiments in a 0.288 diameter column. While maldistribution consequently reduces the gas side mass transfer, the reduced liquid bulk flow weakens the effect of liquid side mass transfer.

Transport Phenomena and Fluid Mechanics

Keywords: Fluid Distribution; Cell Model; Random Packed Column; Mass Transfer; Scale-up

1. Introduction

Liquid maldistribution is a well-known phenomenon in packed columns, which can occur at different intensities, especially in random packings[1]. There are various types of maldistribution in packed columns, which are usually divided into large and small scale maldistribution[2]. The main causes of maldistribution are initial maldistribution[1], e.g. due to inadequate design of the liquid distributor, and maldistribution resulting from the packing itself[3]. The latter include wall flow as a large-scale maldistribution resulting from the anisotropy of the packed bed at the column wall, and small-scale maldistribution that often results from voids or densely packed sections within the packed bed or support structures[2].

Maldistribution is known to reduce separation efficiency in industrial sized columns[4]. In particular, the effect of maldistribution on the characterization of random and structured packings is of great interest since fluid dynamics and mass transfer characteristics are important for column design and scale-up. These parameters determined with laboratory equipment can vary considerably depending on the equipment used and the maldistribution present[5]. For a safe and efficient column design, engineers must rely on the characterized data, which are usually provided by the internal manufacturer. The column is then designed or scaled-up using the data provided and experience-based safety margins for the height of the packed bed[6]. One of the main reasons for uncertainties in the design of packed columns can be attributed to the wall flow affecting the characteristics in laboratory equipment, especially when the column to packing diameter ratio is lower than six[7]. However, even above this ratio a significant wall flow can be observed[8]. To address the topic of maldistribution and its effect on the packed column scale-up, a comprehensive model and parametrization approach is presented, which allows the determination of fluid dynamics and mass transfer in random packed columns influenced by maldistribution. The approach is based on a cell model developed by van Holt[8–12], which is extended by a more detailed representation of the wall flow. A description of the gas distribution, pressure drop and mass transfer is also implemented.

Experimental data obtained with a wire-mesh sensor are used for parametrization of the fluid distribution.

2. Cell models for packed column design

Throughout the history of maldistribution in packed columns, different model approaches have been developed to describe and understand the phenomena of liquid and gas phase distribution. Although there are many different types of models, three different approaches can be distinguished to predict maldistribution: Diffusion models, CFD models and cell models.

The first diffusion model was presented in 1957 by Cihla and Schmidt[13] and consequently has been further investigated in many subsequent studies. Of all approaches, the diffusion model is the most intuitive and can simulate large column volumes up to the industrial scale. However, the level of detail of such models is low and the mechanism of liquid distribution is mostly based on gradients for liquid hold-up or concentration and a diffusion or a spreading coefficient. This is often in contradiction with the idea of continuous liquid mixing, even when a steady distribution is reached.

With the increase in computing power, CFD models are becoming more promising for simulating two-phase countercurrent flow in packed columns. CFD models combine a very high level of detail with a resulting high extrapolation capability. Nevertheless, multiphase CFD approaches are still at a level of validation and the simulation of complex structures is often limited to geometrically periodic structures[14]. Moreover, long computing times are required to calculate large column volumes.

Cell models combine the advantages of the previously discussed approaches by enabling to simulate the entire column while maintaining an appropriate level of detail. Cell models can be applied to evaluate the influence of fluid dynamics and liquid distribution on mass transfer and still allow the implementation of flow phenomena. Different model approaches are available, which can be divided into network models, random distribution models and non-random distribution models.

In 1966 Jameson[15] developed a model approach based on the idea of a cell network at the scale of a packing element that can be transferred into the diffusion equation and also considers wall effects.

The cells are arranged as layers of concentric rings around the center of the column. The flow from each cell is distributed as shown in Figure 1 A by splitting parameters, which were fitted to experimental data of Baker et al.[16]. Herskowitz and Smith[17,18] adapted the approach of Jameson[15] to model liquid flow in trickle bed reactors. To model the wall flow maldistribution, two distribution parameters are used for the bulk and wall cells. The parameters were fitted to experimental flow rates obtained with a liquid collector[17] and tracer distribution experiments[18]. Local liquid flow rates and the concentration profiles were simulated with sufficient accuracy.

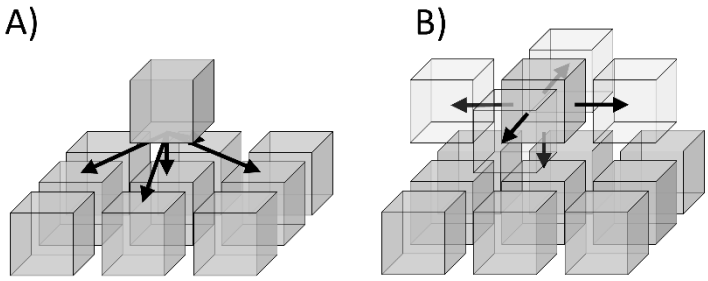

Figure 1: Liquid distribution directions in cell models: A) vertical and diagonal and b) vertical and horizontal direction

The cell model approach developed by Hoek in 1983[2] is based on a random-walk simulation. This type of model is also known as “natural flow models” because liquid distribution is assumed to be a random process. The column is divided in rectangular cell layers with a cell of the size of a packing element. The liquid is described as “spheres”, which can move randomly in the directions indicated by Figure 1 B to describe small-scale maldistribution. A diffusion model was used to describe the large-scale maldistribution. Albright[3] developed a similar random distribution cell model for liquid flow to study the bed depth required for natural flow distribution. The liquid flow in the column cells is divided by half with one half flowing straight downward and the other being distributed to one of the diagonal cells according to Figure 1 A. Wall flow is considered by a redistribution coefficient at the column wall.

Another random distribution approach was introduced by Stikkelman[19]. The cell model is based on a Monte-Carlo distribution mechanism. Similar to the model of Albright[3] and Hoek[2], fractions of the

liquid are distributed according to Figure 1 A. In addition to the liquid flow distribution, Stikkelman also considers the gas distribution. Wall effects are modeled by implementing two different distribution factors for the column wall and bulk.

In 2001, Wen et al.[20] introduced a random walk cell model, but with cell size of 1/10th of the scale of a single packing element. The distribution parameters are calculated by triangulating the real packing surface gradient within the cell. Therefore, a random packed bed and the position of each packing element is simulated using a collision detection algorithm[21].The liquid is distributed according to Figure 1, B. The model is in good agreement with experimental data without the need of experimental distribution coefficients.

A different random distribution approach was presented in 2007 by Wild and Engel[22] and further developed by Wild et al.[23] and Hanusch et al.[24,25]. The model consists of hexagonal cells with the size of a packing element from which the liquid can flow straight and diagonally downward into the seven adjacent cells. A set of distribution coefficients for each adjacent cell was obtained from virtual irrigation experiments of CAD random packing models for a total of seven spatial packing positions. The sets of distribution parameters for all directions were randomly applied to the cells to describe the liquid distribution as realistically as possible. Liquid hold-up and pressure drop were implemented based on a fluid dynamic correlation. Wall flow was achieved with a reduction of the distribution parameters in the wall cells by a random number between 0 and 1 to account for the decrease in porosity at the wall. The model was validated against a variety of random packings and initial distributions with reasonably good agreement between measured and simulated liquid flow profiles within a range of 50 % accuracy.

Zuiderweg et al.[26,27] developed the first model for predicting the mass transfer, taking into account the influence of liquid maldistribution, but not the random behavior of the liquid. The model is known as the zone/stage model and was applied for random and structured packings. Different geometric approaches were realized, e.g., annular rings, ring segments and rectangular cells with cell sizes greater than a single packing element. The height of each stage was chosen as the HETP of the

packing for ideal irrigation. The liquid distribution is calculated by applying a splitting factor, which was obtained from the spreading coefficient determined for the diffusion models. Different splitting factors are applied for wall and bulk cells. The liquid is distributed according to Figure 1 A. Mass transfer was successfully determined for a variety of cases based on the simulated liquid distribution profiles. In 1997, Song et al.[28] modified this approach by adding random flow directions as well as random flow fractions from one cell to the adjacent, transferring this approach in a random distribution “natural flow”. Higler et al.[29] also extended the mass transfer approach of the zone/stage model by a non-equilibrium approach, considering the chemical potential in each cell.

Using cross-sectional temperature profiles for model verification, Potthoff[30] and Schneider[31] investigated a cell model approach with hexagonal cell layers and concentric ring segments at the column wall. Plug flow is assumed within each cell and the exchange of the fluids between the cells is calculated depending on the diffusion coefficient, which is determined by the already mentioned diffusion model approach. The geometry differences between bulk and wall cells are calculated on the base of the cell side areas. The cell includes several packing elements since the cell number is fixed in this model approach. The liquid is distributed as shown in Figure 1 A, using two distribution parameters for wall and bulk cells. Mass transfer was realized based on the HTU-NTU concept. Kammermaier[32] further developed this approach by implementing additional distribution element zones as well as anisotropic distribution parameters with an increased liquid distribution towards the wall.

Recently, van Holt et al.[8–12] introduced a non-random cell model approach for prediction of the liquid distribution and the scale-up of packed columns, which focuses on the wall flow. The approach is similar to the zone/stage model by Zuiderweg[26,27] with variable cell sizes depending on the chosen segmentation. Instead of complete rings, the column is divided into concentric ring segments and the liquid is distributed according to Figure 1 B. Cell hold-ups are determined as a function of the liquid distribution using a common literature correlation. Van Holt determined the distribution parameters from measurements with a wire-mesh sensor. The simulation results and experimental data were in

good agreement at low liquid loads but deviate at higher ones. Scale-up was performed by an increase of the cell number. The simulation results for a scaled-up column filled with Pall Ring 25 M were shown to be in reasonably good agreement with experimental data of Kouri and Sohlo[33].

3. Modeling fluid maldistribution in packed columns

3.1 Model structure and fluid distribution mechanism

The goal of this publication is to present a model approach that focuses on large-scale maldistribution. On the one hand, the influence of wall flow on fluid dynamics and mass transfer during characterization and scale-up is described with high accuracy to allow a more detailed description of local mass transfer in wall and bulk zones of the packed column. On the other hand, the effect of initial maldistributions can be addressed by the application of different liquid distributor designs. The model of van Holt et al.[8–12] is chosen as a basis, because first promising scale-up results were achieved.

In contrast to the previous model, where scale-up is done by increasing the number of cells, this model is intended to operate at a constant cell number. Scale-up is performed by adjusting the distribution parameters to the larger geometry. This was found to be advantageous, because the adaption of the distribution coefficients to experimental data can be done with a high spatial resolution at a chosen computational effort. The computational effort then does not change during scale-up, because the number of equations is kept constant at the expense of decreasing spatial resolution. The process of parameter adjustment and scale-up is described in chapter 4.

As displayed in Figure 2, polar coordinates are chosen for cell geometry. The model consists of several layers of concentric ring segments. The fluid is distributed vertically into the next cell layer ($\dot{V}_{out,down}$¿ as well as radially in the adjacent cells ($\dot{V}_{out,side}$¿. Thus, increased mixing, that occurs at loading and flooding conditions, can be described within the same cell layer. The liquid distribution is modeled by a distribution coefficient k_i based on the idea of a single random packing element shown

in Figure 3 A. The distribution coefficient is defined as the ratio between lateral flow $\dot{V}_{side,packing}$ and total flow $\dot{V}_{out,packing}$ as given by equation (1).

$$k_i = \frac{\dot{V}_{side,packing}}{\dot{V}_{out,packing}} = \frac{\dot{V}_{side,packing}}{\dot{V}_{down,packing} + \dot{V}_{side,packing}} \quad (1)$$

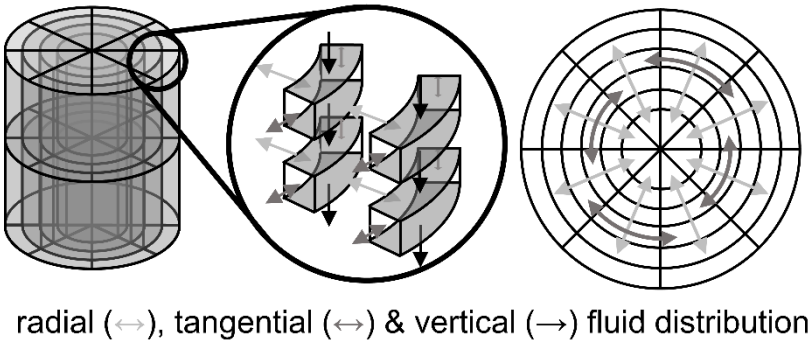

Figure 2: Model geometry and liquid distribution directions

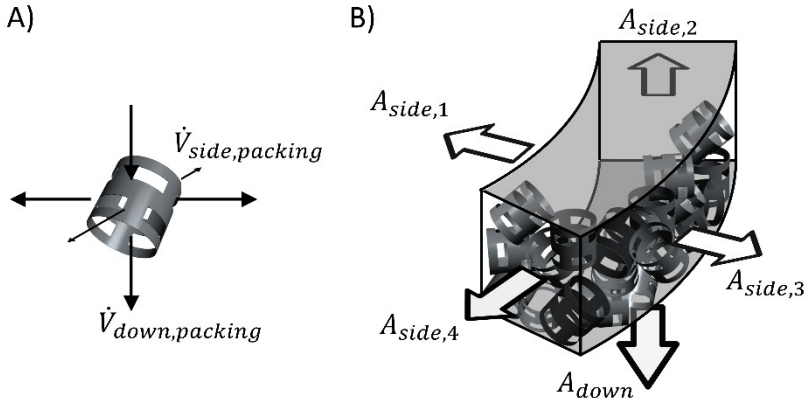

Figure 3: Distribution direction of A) a single packing element and B) cell side areas for liquid flow

The flow behavior at the wall differs from that in the bulk. Inside the column bulk, a strong mixing between liquid films and rivulets takes place, while interactions in the wall region are lower due to less contact points between the packing elements and the wall. Most of the liquid flows straight down the wall and only a small fraction is redistributed into the bulk by adjacent packing elements. Therefore, two distribution parameters k_i are used for the bulk k_{bulk} and the wall k_{wall}.

The transition from the single packing element to the cell geometry is done by area weighting with the respective side surfaces $A_{side,j}$ and A_{down} according to equations (2) to (4) or Figure 3 B. According

to equation (5), constant liquid spreading is achieved by a constant cell width in radial direction and a scaling factor *w* in tangential direction, shown in in equation (5). The factor *w* relates the cell width r_j - $r_{j-1}$to the average circumference $\pi\ n_{tg}^{-1}(r_j + r_{j-1})$ of a cell. This depends on the outer and inner cell radius r_j and r_{j-1} and the number of cells in the tangential direction n_{tg}.

$$\dot{V}_{out,down} = \frac{(1-k_i)\cdot \dot{V}_{out,packing}\cdot A_{down}}{(1-k_i)\cdot A_{down} + \sum_{j=1}^{4} k_i \cdot A_{side,j}} \tag{2}$$

$$\dot{V}_{out,side,j} = \frac{k_i \cdot \dot{V}_{out,packing}\cdot A_{side,j}\cdot w}{(1-k_i)\cdot A_{down} + \sum_{j=1}^{4} k_i \cdot A_{side,j}} \tag{3}$$

$$\dot{V}_{out} = \dot{V}_{out,down} + \sum_{j=1}^{4} \dot{V}_{out,side,j} \tag{4}$$

$w = 1$ for radial cell sides; $w = \frac{r_j - r_{j-1}}{\frac{2\pi}{n_{tg}}\frac{r_j + r_{j-1}}{2}}$ for tangential cell sides (5)

With this definition, a constant liquid spreading, as usually observed in distribution experiments, can be achieved, which is linear with respect to the column height and the reciprocal of the column diameter. This linear dependency eases adaption of the parameters to scaled-up column dimensions.

Gas distribution is chosen in analogy to the liquid distribution. While experimental coefficients are necessary for liquid distribution, gas distribution coefficients could not be determined sufficiently by experiments. Therefore, an approach presented by Duss[34] was adapted, which assumes the local gas flow in such a way that the local pressure drops are constant across the cell layer. Furthermore, it was assumed that gas distribution is proportional to ratio of gas load and flooding point $F_V \cdot F_{V,FL}^{-1}$ with a maximum in gas mixing at the flooding point. Equation (6) represents this approach, with the first part being responsible for the equalization of the local pressure drops in the cell layer. The exponent A has to be chosen high enough to reduce the deviation between the pressure drop of the cell and the cell layer to a predefined accuracy, but low enough to avoid solution problems of the numerical solver. In this work, the gas exponent is chosen to be < 50, resulting in pressure gradients < 1 Pa

across the different cell layers. While bulk and wall cells are treated separately, no differentiation was made between wall and bulk cells for the gas distribution, because gas distribution is linked to the liquid distribution via the local liquid loads.

$$k_{gas}=\left[\frac{\left(\Delta p\cdot H^{-1}\right)_{cell}}{\left(\Delta p\cdot H^{-1}\right)_{layer}}\right]^{A}\left(\frac{F_V}{F_{V,Fl}}\right) \tag{6}$$

For each cell the mass and molar conservation equations (7) and (8) are solved for the liquid phase, where $H_{L,cell}$ is the liquid cell hold-up, V_{cell} and c_{cell} the geometric cell volume and cell concentration, $\dot{V}_{¿}$ and $\dot{V}_{out}$ the incoming and outgoing flows and $c_{¿}$ and c_{out} the respective concentrations. Gas flow was assumed to be incompressible over the column height, which leads to the conservation equations (9) to (11), where $\dot{G}_{¿}$ and $\dot{G}_{out}$ are the incoming and outgoing gas volume flows, H_G the gas hold-up and $y_{¿}$ and y_{out} the corresponding fractions of the transferred component for which ideal gas behavior is assumed.

$$\frac{dH_{L,cell}}{dt}V_{cell}=\sum\dot{V}_{¿}-\sum\dot{V}_{out} \tag{7}$$

$$\frac{d\left(H_{L,cell}V_{cell}c_{cell}\right)}{dt}=\sum\dot{V}_{¿}c_{¿}-\sum\dot{V}_{out}c_{out}+\dot{n}_{flux} \tag{8}$$

$$\sum\dot{G}_{¿}-\sum\dot{G}_{out}=\dot{G}_{flux} \tag{9}$$

$$H_G=\left(1-H_L\right) \tag{10}$$

$$\sum\dot{G}_{¿}y_{¿}-\sum\dot{G}_{out}y_{out}=\dot{n}_{flux} \tag{11}$$

The transferred molar amount $\dot{n}_{flux}$ between gas and liquid is calculated by the mean logarithmic concentration gradient according to equation (12) with k_{OL} as the liquid based volumetric mass transfer coefficient, *x* and *y* m_{yx}^{-1} as the molar fractions and the equilibrium molar fraction of the cell outlet and the cell inlet.

$$\dot{n}_{flux}=k_{OL}aV_{cell}\frac{\left(y_{cell}\cdot m_{yx}^{-1}-x_{¿}\right)-\left(y_{¿}\cdot m_{yx}^{-1}-x_{cell}\right)}{\ln\left(\frac{y_{cell}\cdot m_{yx}^{-1}-x_{¿}}{y_{¿}\cdot m_{yx}^{-1}-x_{cell}}\right)} \tag{12}$$

3.2. Cell characteristics: Hold-up, pressure drop and mass transfer

As mentioned before, the bulk cell characteristics, including the liquid hold-up, the pressure drop and the mass transfer parameters, are calculated by means of correlations. However, instead of constant gas loads, loading points and flooding points as applied in the original model, in the present version, local values are calculated for each cell. Since no correlations are available to describe the local characteristics, the set of integral correlations by Billet und Schultes[35] was implemented for local fluid dynamics and mass transfer. First, the local gas loads for loading and flooding are calculated considering the local liquid loads. The latter is defined by the axial flow from the overlying cell and the cell surface area in axial direction. On this basis, hold-up, pressure drop and mass transfer parameters are calculated iteratively considering the local liquid and gas loads of each cell.

As in reality, the flow behavior at the column wall differs from that in the bulk. Instead of hold-up correlations, the film flow at the column wall is approximated with the film flow theory according to Nusselt[36], which also is the basis for the Billet and Schultes[1] correlation The film thickness δ in each cell i can therefore be calculated by equation (13) as a function of the local liquid load $u_{L,i}$ at the column wall, the liquid viscosity η_L, the density ρ_L and the specific surface area a. The wall cell hold-up is defined by the given film thickness, which then requires a constant wall cell size, independent of the column diameter. Changing the wall cell width would influence the hold-up and consequently the pressure drop. This would contradict the expectation that a wall film of known thickness would also result in the same wall pressure drop, independent of the column geometry. Moreover, a smaller wall region is expected for smaller packings. Therefore, the ratio of wall area to wall cell volume was assumed to be equal to the specific packing surface, which is unique to each type of packing and usually increases with decreasing packing size. The resulting cell width Δr_{wall} can be calculated using equation (14).

$$\delta_i^3 = 3\frac{u_{L,i}\eta_L}{a\rho_L g} \tag{13}$$

$$a = a_{wall} = \frac{wall\,area}{cell\,volume} = \frac{2\pi R}{\pi\left[R^2 - \left(R - \Delta r_{wall}\right)^2\right]} \approx \frac{1}{\Delta r_{wall}} \tag{14}$$

Again, the Billet and Schultes[35] correlation is used in a modified form for the wall cells to approximate loading, flooding, pressure drop and mass transfer parameters. In contrast to the bulk cells, phase inversion is neglected for the calculation of the flooding point in the wall region, since observations of the flow at the column wall have shown that the liquid almost completely flows within the wall film and the gas is maintained as the continuous phase until flooding is reached.

The effective interfacial area a_{eff} in the wall cells is approximated the mass transfer area of the packing and the area of the wall according to equation (15), because it is expected that both interfacial areas are present in the wall region. The specific interfacial area at the wall $(a_{eff} \cdot a^{-1})_{wall}$ can have values ≤ 1, which considers incomplete wetting of the wall at low liquid loads. For complete wetting, the interfacial area of the wall is limited to a value of 1. The wetting of the wall is approximated by the ratio of the wall-specific liquid load and the critical load of 0.5 – 1.5 $m^3m^{-1}h^{-1}$, which according to Kraume[36] is associated with complete wetting. For this work, a critical wall-load of 0.5 $m^3m^{-1}h^{-1}$ is in good agreement for the film flow observed in the used PVC column. In case of a wetted wall, it can be assumed that the packing inside the wall cells is also wetted. Therefore, the effective phase interface $(a_{eff} \cdot a^{-1})_{Billet\ \&\ Schultes}$ in the wall cells is also included. Due to equation (14), this leads to an effective phase interface larger than a (or $a_{eff} \cdot a^{-1} > 1$). For a partially wetted wall below the critical wall-load of 0.5 $m^3m^{-1}h^{-1}$, the wall cell region is also assumed to be only partially wetted. Thus, the interfacial area of the packing $(a_{eff} \cdot a^{-1})_{Billet\ \&\ Schultes}$ is scaled with the effective area at the column wall $(a_{eff} \cdot a^{-1})_{wall}$.

$$\frac{a_{eff}}{a} = \left[1 + \left(\frac{a_{eff}}{a}\right)_{Billet \wedge Schultes}\right]\left(\frac{a_{eff}}{a}\right)_{Wall} \tag{15}$$

A comprehensive visualization of the applied correlations for bulk and wall cells is shown in Figure 4.

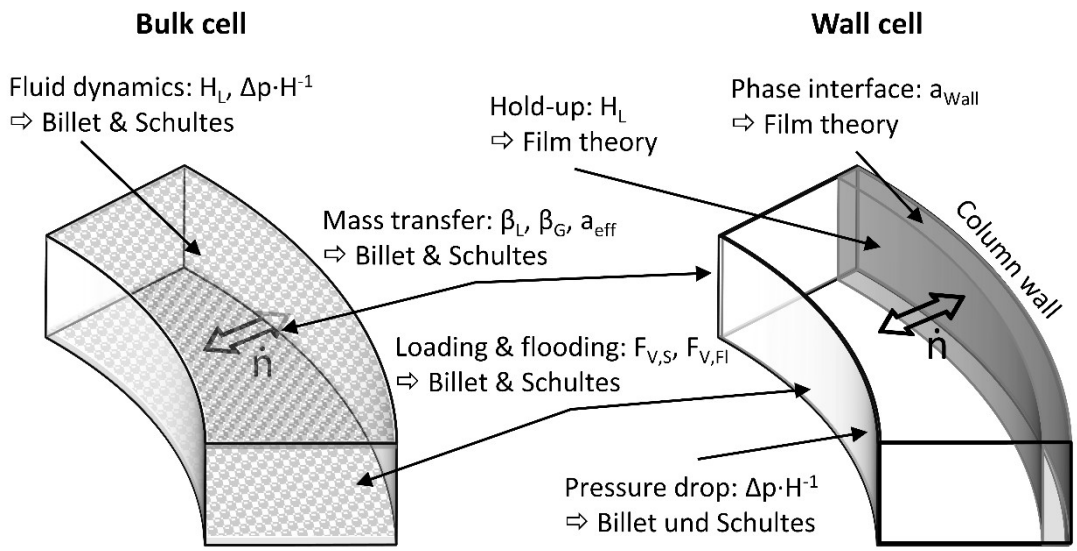

Figure 4: Fluid dynamic and mass transfer correlations applied for bulk and wall cells

3.3 Dynamic flow in packed beds

The dynamic of the flow within the packed bed is modeled with an adaption of Torricelli's' law according to equation (16). For the local liquid loads, hold-ups, loading and flooding conditions it was found that the initially chosen dynamic expression given by equation (17) leads to fluctuations. These can be attributed to differences in the potential hold-ups $H_{L,cell,pot}$ between bulk and wall cells for non-uniform initial liquid distributions. $H_{L,cell,pot}$ is the calculated hold-up by the Billet & Schultes correlation for the local liquid and gas loads present. $H_{L,cell}$ is the actual cell hold-up that consequently changes due to the local loads until it approaches $H_{L,cell,pot}$.

$$\dot{V}_{out} - \dot{V}_{¿} = H_{L,cell} A_{cell} \sqrt{2g \frac{H_{L,cell}}{a}} - H_{L,cell,pot} A_{cell} \sqrt{2g \frac{H_{L,cell,pot}}{a}} \tag{16}$$

$$\dot{V}_{out} = \sqrt{\frac{H_{L,cell}}{H_{L,cell,pot}}} \dot{V}_{L,\in ¿¿} \tag{17}$$

The outflow of each cell is defined as a function of the liquid hold-up and the axial cell area, which represents the free flow cross-section of the liquid. The expression corresponding to the liquid height in Torricelli's law below the square root is chosen in dependence of the hold-up H_L and the specific packing surface a. The reciprocal of the specific packing area a was chosen as the liquid height in the cells, because with an increase in the specific surface area of the packing, the hold-up is distributed

more evenly on the packed bed surface. This leads to thinner films and thus to a reduction of the flow velocity over the packing surface.

4. Model parametrization

The model is parameterized by fitting the distribution parameters k_{wall} and k_{bulk} to normalized experimental data obtained with a wire-mesh sensor by van Holt[8] in a column of D = 0.288 m inner diameter. The data were re-evaluated to obtain signal profiles across the cross-section of the column. Water-air experiments were performed with continuous sodium chloride tracer injection in the center of a packed bed with a height of H =0.5 m and on the column wall at a packed bed height of H =1.5 m. The wire-mesh sensor was operated in conductance mode directly below the packing. The profiles were obtained during stationary operation of the packed column. A detailed description of the experimental setup is given by van Holt[8].

4.1 Wire-mesh sensor signal

As the wire-mesh sensor does not measure common variables such as concentration or volume flow rates, the sensor signal was recreated within the model to allow parameter determination using the experimental signals. In analogy to a conductivity cell, the sensor-signal (analog digital converter) is dependent on the conductance and therefore on the concentration c and the area A_{flow} of the liquid flow. Latter can be described as a function of the volume flow rate $\dot{V}$ and the average velocity $\bar{u}$of the liquid flowing through the sensor. Due to the differences in velocity of the film flow at the column wall and the free-falling droplets below the packing in the center of the column, wall and bulk signals cannot be compared to each other by means of concentration or volume flow rate only. While a constant signal is obtained at the wall due to the continuous film flow, the droplets in the bulk of the column fall through the sensor at a higher average velocity creating a discrete signal. The average velocity of the liquid at the wall is approximated with the film thickness for a given wall flow rate using the Nusselt-film-theory. The velocity of the droplets in the bulk was calculated as a free-falling sphere with air resistance. The required droplet diameter was determined experimentally. Therefore, the number of drops and the corresponding total volume was measured for about 100 s at different bed positions. The diameter was found to be between 6.1 and 6.7 mm with a mean droplet diameter of 6.44 mm. These results are in good agreement with the maximum droplet size of 6.65 mm as predicted by Maćkowiak[37].

$$signal = f\left(c \cdot A_{flow}\right) = f\left(c \cdot \dot{V} \cdot \bar{u}^{-1}\right) \tag{18}$$

Another factor to consider when calculating the sensor-signal is the signal loss due to the spherical shape of the droplets. While the film at the column wall is completely detected, the spherical shape of the droplet leads to a time dependent conductance signal. Therefore, calculations for the conductance signal of a falling sphere with the determined mean droplet size were performed. The conductance signal was calculated from the time-dependent, mean cross-sectional area of the drop, the given distance between the wire layers of the wire mesh sensor of 3 mm and the possible spatial drop positions. It was found that droplets passing the sensor result in an average of 51.7 % of the

signal that a film with the same volume and concentration would cause. The simulated sensor-signals for the bulk were additionally reduced by this factor. The final signals for bulk and wall cells are calculated according to equation (19) and (20), where $H_{L,wall}$ is calculated by the film thickness δ.

$$bulk\ signal = 0.517 \cdot c_{bulk} \cdot \dot{V}_{bulk} \cdot \bar{u}_{bulk}^{-1} \tag{19}$$

$$wall\ signal = c_{wall} \cdot \dot{V}_{wall} \cdot \bar{u}_{wall}^{-1} = c_{wall} \cdot \dot{V}_{wall} \cdot u_{L,wall}^{-1} \cdot H_{L,wall} \tag{20}$$

4.2 Parametrization and parameter scale-up procedure

The parametrization and scale-up of the model are done in the five steps visualized in Figure 5. Parameters are fitted for a column with constant cell number of 32 radial rings, 8 tangential segmentations and 20 axial cell layers.

First, the parameter k_{bulk} is determined from liquid spreading experiments with central tracer injection (Step 1). This is done by fitting the measured distribution profiles below a packed bed of 0.5 m height as shown in Figure 6 A. The height of 0.5 m was chosen to ensure that no tracer reached the column wall. Thus, the spreading is not influenced by the wall and k_{bulk} is independent of k_{wall}. Before fitting k_{wall} to match the experimental data of the wall tracer injection experiments, the parameter k_{bulk} was adjusted to the packed height of 1.5 m (Step 2). Since the cell number is kept constant, this step is required to compensate for the change in distribution due to the changing cell size. Therefore, k_{bulk} is adjusted to ensure that the concentration profiles at a certain axial cross-section within the packed bed are identical. In step 3, k_{wall} is determined from the distribution profiles of the tracer injected at the column wall (Figure 6 B). In contrast to k_{bulk}, the determination of k_{wall} strongly depends on the bulk distribution parameter k_{bulk}.

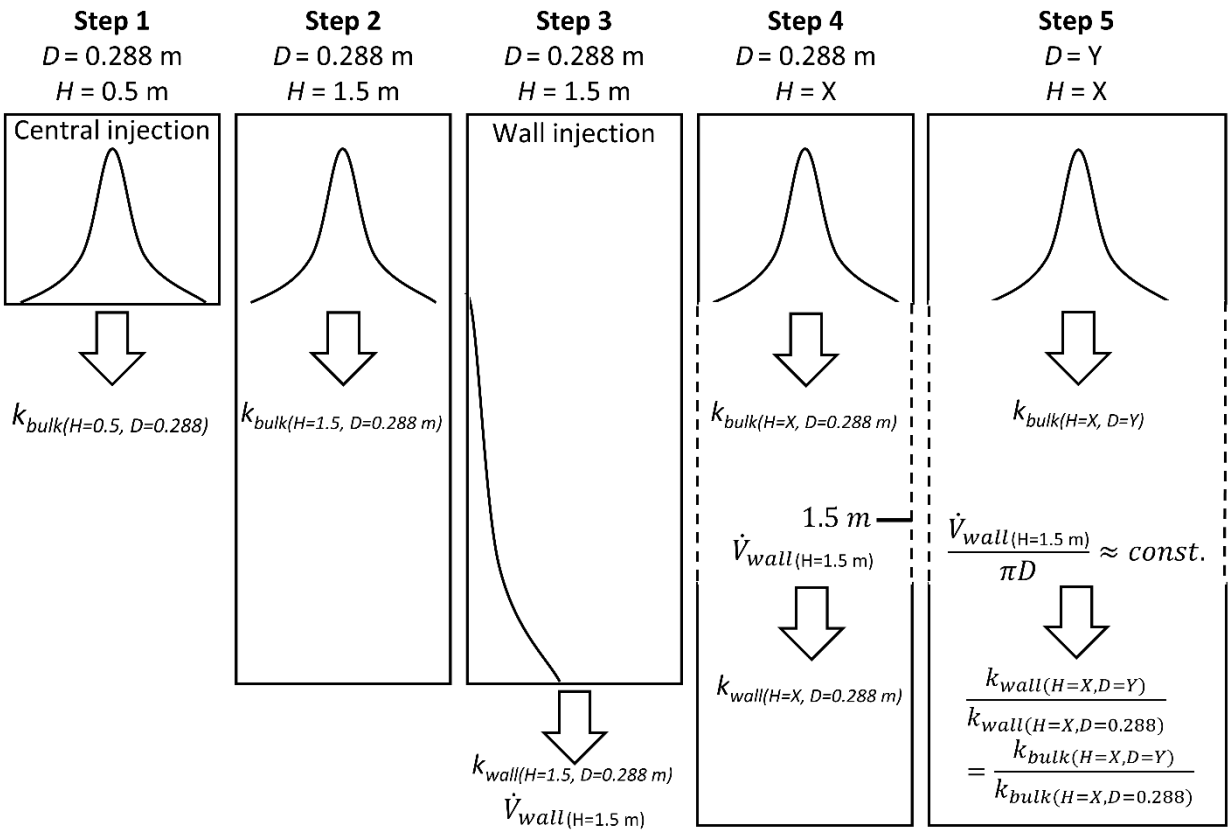

Figure 5: Schematic parameter scaling procedure for column scale-up

Step 4 describes the scale-up of the column height, which is identical to step 2 for k_{bulk}. In analogy to k_{bulk}, k_{wall} must also be adjusted with the change of the cell height. This is realized by ensuring that the wall flow remains identical after a certain packed height H, regardless of the cell height. Finally, in step 5, the scale-up of the column diameter is presented. As in steps 2 and 4, k_{bulk} is adapted to the concentration profile at a certain packed height. Since the wall flow depends on the flow towards the wall, determined by k_{bulk}, and the flow away from the wall, determined by k_{wall}, a change in k_{bulk} due to a different cell geometry also requires an adjustment of k_{wall}. It follows from the distribution mechanism that the formation of the wall film is expected to be independent of the column diameter, and thus the volumetric flow per wall circumference can be approximated as constant. This is achieved by a simple ratio scaling of the distribution parameters according to equation (21).

$$k_{wall(D=X)} = \frac{k_{bulk(D=X)}}{k_{bulk(D=0.288)}} k_{wall(D=0.288)} \tag{21}$$

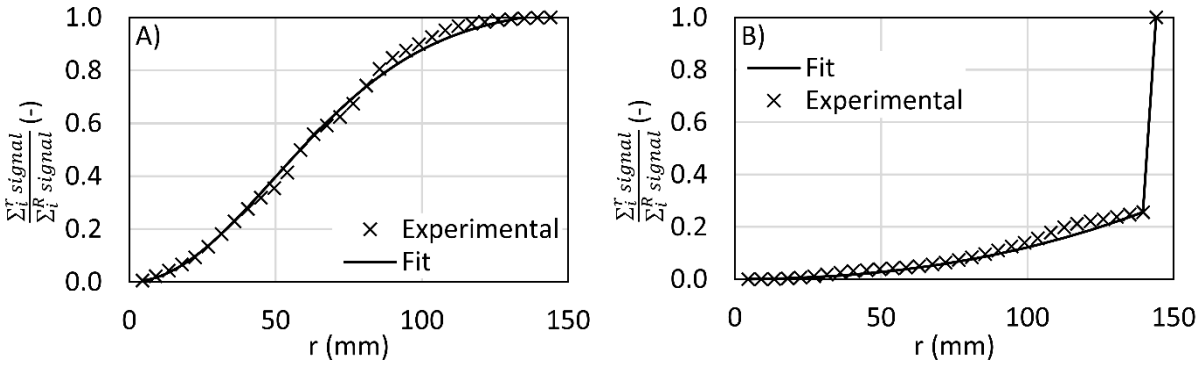

Figure 6: Typical normalized experimental cumulative sensor-signal profiles and model fit at u_L = 40 $m^3\ m^{-2}h^{-1}$ and F_V = 0.99 $Pa^{0.5}$ for A) central tracer injection and B) wall tracer injection

The resulting distribution parameters for bulk and wall at their specific experimental packed bed height are shown in Figure 7. Due to the independence of the liquid flow from the gas flow below the loading point, a constant profile is observed. On the other hand, above the loading point an increase of both distribution parameters is found due to rising interactions between gas and liquid flow. For the bulk distribution, an increase of k_{bulk} results in a wider spreading of the tracer. A higher k_{wall} reduces the liquid flow at the wall and therefore the fraction of the signal at the column wall, since more liquid is exchanged from the wall to the bulk of the column. Both parameters are independent of the liquid load within a range of 20 %, which is consistent with literature[19,38–40].

The observed distribution behavior was found to show a similar dependence from the gas load as usually observed for the hold-up. Based on this, k_{bulk} and k_{wall} were correlated with the gas load according to the approach applied by Billet and Schultes[35] for the liquid hold-up given by equation (22) and (23). The correlated parameters agree with the experimental parameters within a range of 20 %. The deviations for k_{bulk}, which also influence k_{wall}, can be attributed to the experimental profiles along the column radius, which sometimes show deviations from the normal distribution due to local flow phenomena such as liquid channeling.

$$k_{bulk}\left(F_V \cdot F_{V,Fl}^{-1}\right) = k_{bulk,F_V<F_{V,S}} + \left(k_{bulk,F_{V,Fl}} - k_{bulk,F_V<F_{V,S}}\right)\left(\frac{F_V}{F_{V,Fl}}\right)^{13} \tag{22}$$

$$k_{wall}\left(F_V \cdot F_{V,Fl}^{-1}\right) = k_{wall,F_V<F_{V,S}} + \left(k_{wall,F_{V,Fl}} - k_{wall,F_V<F_{V,S}}\right)\left(\frac{F_V}{F_{V,Fl}}\right)^{13} \quad (23)$$

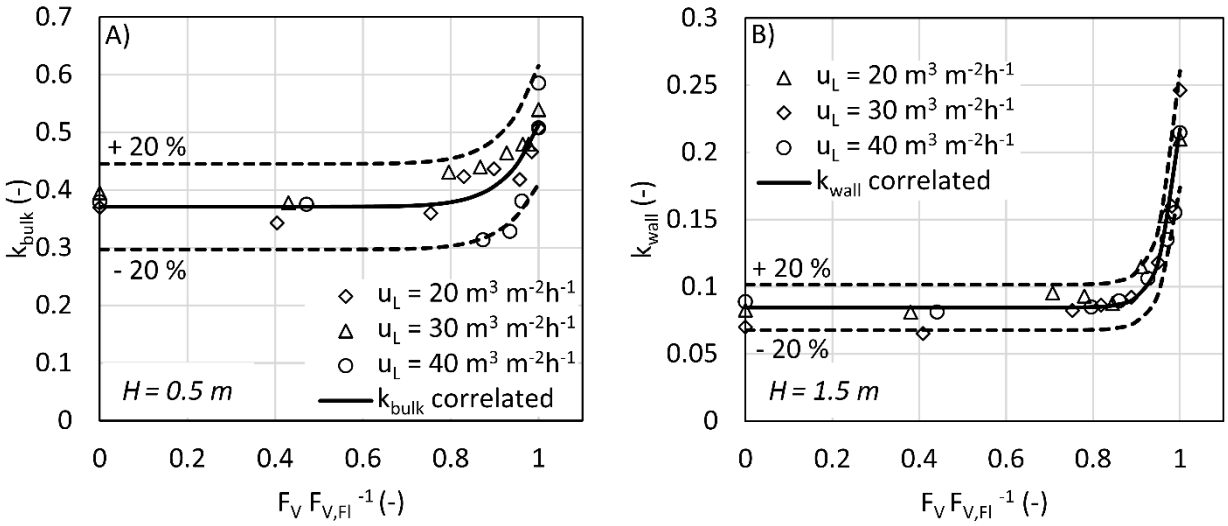

Figure 7: Model distribution parameters determined from the experimental data for A) bulk and B) wall tracer injection

5.Model validation and simulation-based packed column design

Simulations for model validation and scale-up performance were conducted with the experimentally determined parameters from 4.2, which were scaled to the simulated geometries using the procedure presented in 4.1. Simulation results are compared with the correlation of Billet and Schultes[35] and with experimental data of the fluid dynamics, liquid distribution and mass transfer measurements. The experiments were conducted in a column with an inner diameter of D = 0.288 m and a packed bed height H = 1.5 m according to VDI 2761/2[7]. All experiments were performed with water and air. The liquid-side mass transfer was measured by CO_2 desorption. The combined gas and liquid-side mass transfer was determined by ammonia absorption. The scale-up capability of the model approach is validated with literature data for the Pall Ring 25 M at different column diameters and heights. Where applicable, the liquid distributor inlet profile was applied for all simulations. The physical properties used for correlation and simulations are listed in Table 1.

Table 1: Physical properties in this work at T = 290.15 K

Property		Value	Reference
ρ_L	kg m^{-3}	998.78	[41]
η_L	Pa s	1.08 10^{-3}	[41]
σ_L	kg s^{-2}	0.07319	[41]
$D_L(CO_2)$	m^2 s^{-1}	1.59 10^{-9}	[42]
$D_L(NH_3)$	m^2 s^{-1}	1.72 10^{-9}	[1]
M_L	kg mol^{-1}	0.018	[43]
ρ_G	kg m^{-3}	1.192	[43]
η_G	Pa s	1.79 10^{-5}	[41]
$D_G(CO_2)$	m^2 s^{-1}	1.58 10^{-5}	[44]
$D_G(NH_3)$	m^2 s^{-1}	2.38 10^{-5}	[1]
M_G	kg mol^{-1}	0.02895	[43]
$m_{yx}(CO_2)$	mol m^{-3} (mol m^{-3})$^{-1}$	1346.77	[45]
$m_{yx}(NH_3)$	mol m^{-3} (mol m^{-3})$^{-1}$	0.6378	[45]

5.1 Fluid dynamics

The simulated, correlated, and measured hold-up profiles are compared in Figure 8 for a liquid load of u_L = 20 m^3 $m^{-2}h^{-1}$ and u_L = 40 m^3 $m^{-2}h^{-1}$. Compared to the hold-up, predicted by the correlation, the simulated profile is significantly lower for both liquid loads, because with increasing wall flow, bulk flow, and thus liquid hold-up decreases. Therefore, the integral hold-up predicted by the correlation is higher than the simulated. In addition, the increase of liquid hold-up, starting from the loading point, is less sharp compared to the correlation. This effect can be related to the lower bulk hold-up and the way the gas distribution is modeled. A higher local hold-up increases the flow resistance for the gas, which would result in a higher cell pressure drop considering the case that the gas is not distributed. Since it was assumed that the local cell pressure drop is equal across the whole cell layer, the gas flow is distributed to cells with a lower pressure drop. This leads to lower local gas loads in cells with higher liquid hold-up and therefore a delay in reaching the loading condition.

In comparison to the experimental results, the simulated hold-ups correspond well to each other. The mean relative deviation between simulation and experiment is below 8 % for all liquid loads. The

presented model is therefore able to describe local hold-ups for the investigated Pall Ring 25 M very well, while the Billet and Schultes correlation itself shows higher deviations. This indicates that the correlation might be adapted to experimental data obtained from larger column diameters, where wall flow has less influence on the integral values. Nevertheless, these results show how significant the influence of maldistribution on packing characteristics can be, even at the scale of a pilot plant. The correlations usually assume liquid plug flow and neglect distribution influence.

The specific pressure drop profiles in Figure 9 are obtained in the same way as the hold-up for correlation, simulation, and experiments. Due to maldistribution, the pressure drop is lower for the simulation when compared to the correlation. The agreement between simulation and experiments is good below the loading point with a relative mean deviation of 6 %. This is expected due to the strong dependence of the pressure drop on the hold-up. However, above the loading point, the simulated profile starts to deviate with increasing gas loads up to an error of 56 % for u_L = 40 $m^3\ m^{-2}h^{-1}$ at the flooding point. This indicates that gas maldistribution can be described quite well by the chosen approach below the loading point, but above the loading point a more precise local pressure drop calculation is required. The deviation might be attributed to the empirical nature of the pressure drop correlation of Billet and Schultes above the loading point. Nevertheless, it was found that the simulated pressure drops are still in reasonably good agreement to the experimental data, especially when the influence of liquid maldistribution must be considered. It is known that liquid maldistribution reduces the pressure drop. However, this effect has to be evaluated with experiments at different packed bed heights and diameters, if not modeled. Therefore, the presented model is a useful tool to estimate the influence of maldistribution on the pressure drop.

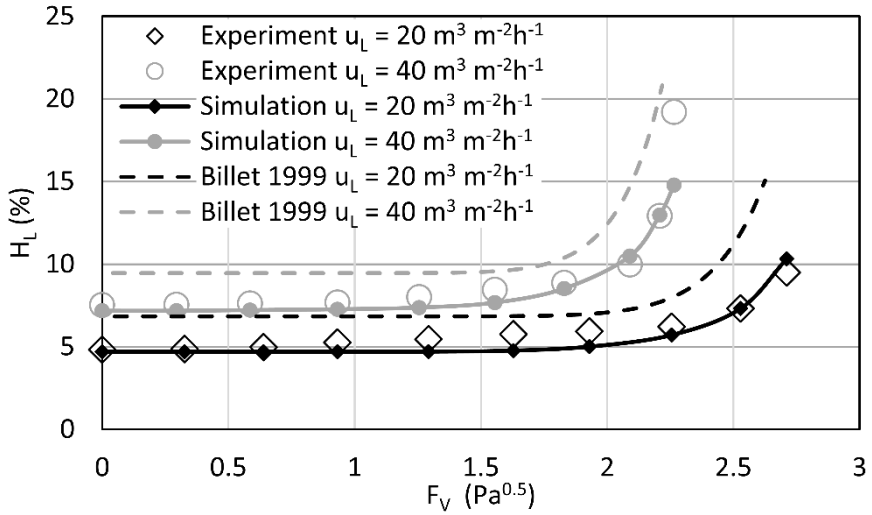

Figure 8: Comparison of liquid hold-ups for simulation, correlation, and experiment

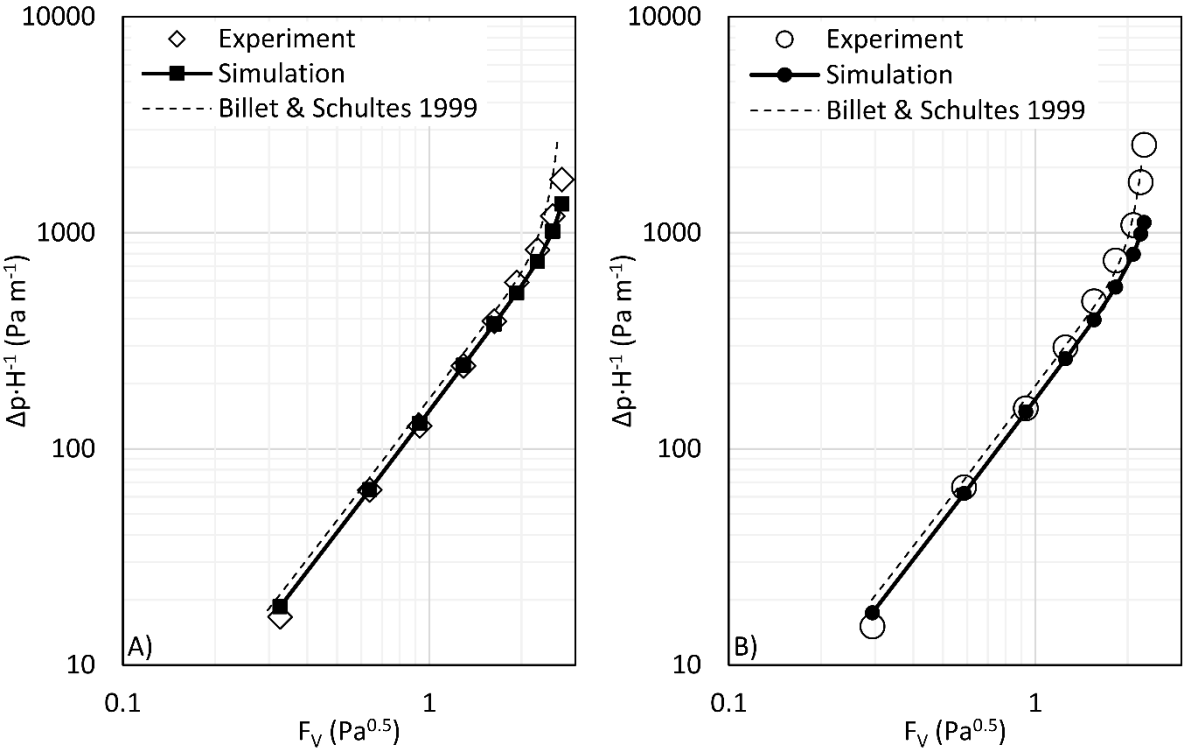

Figure 9: Comparison of pressure drops for simulation, correlation, and experiment at H = 1.5 m for A) u_L = 20 m³ m⁻²h⁻¹ and B) u_L = 40 m³ m⁻²h⁻¹

5.2 Liquid distribution and scale-up

The ability of the model to predict the liquid distribution in packed columns will be validated for different column diameters using experimental data of van Holt[8], Kouri and Sohlo[33] and Sun et al.[46].

The applied distribution parameters for different column diameters and packed bed heights are listed in Table 2.

Table 2: Distribution parameters determined in this work for different diameters and packed bed heights

Diameter D	Packed bed height H	$k_{bulk}(F_V < F_{V,S})$	$k_{wall}(F_V < F_{V,S})$	$k_{bulk}(F_{V,Fl})$	$k_{wall}(F_{V,Fl})$
0.288 m	1.5 m	0.4014	0.0846	0.5441	0.2171
0.288 m	2 m	0.4138	0.0901	0.5600	0.2284
0.5 m	2 m	0.2918	0.0622	0.4230	0.1726
0.5 m	3 m	0.3004	0.0648		
0.6 m	3 m	0.2565	0.0544		

As shown in Figure 10 for a column diameter of 0.288 m, the measured and simulated wall flow fractions are in good agreement. 30 % wall flow already occurs after a length of 0.5 m. Then the increase in wall flow is less rapid up to a packed bed height of 1.5 m. The model therefore not only agrees with the amount of wall flow at a certain height, but also with the development of the wall flow along the height of the packed bed. Although there is some scatter in the experimental results, the simulated wall flow is independent of the liquid load. As mentioned in section 4.2, this in good agreement with general observations from literature. The wall flow development shown in Figure 11 was also found to be valid with the experimental data of the Pall Ring 25 P of Kouri and Sohlo [33] for different packed heights, gas loads and a liquid load of u_L = 18 $m^3\ m^{-2}h^{-1}$.

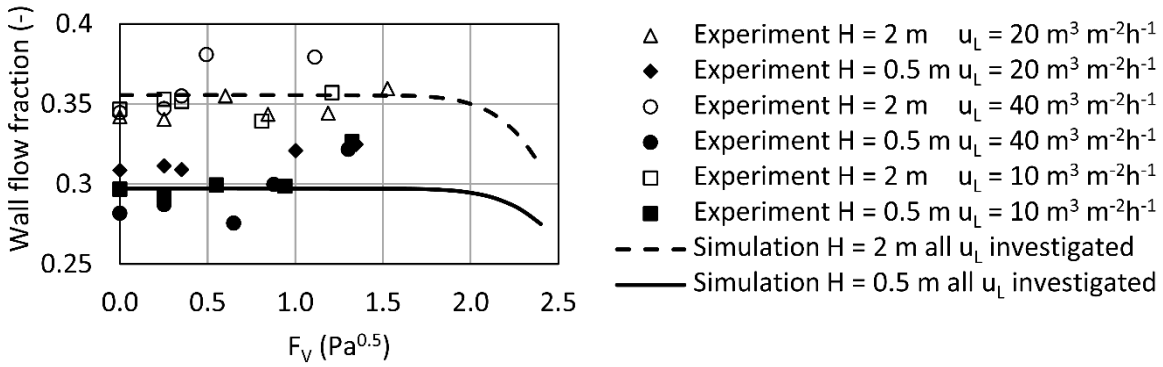

Figure 10: Comparison of simulated and experimental wall flow by van Holt[8] in a packed column of D = 0.288 m

Figure 11 also shows the influence of the liquid distributor profile at the top of the column. For a liquid distributor similar to Kouri and Sohlo with 382 irrigation points per square meter, the development of liquid wall flow is smaller at lower packed bed heights. This can be explained by the fact that liquid drip points are evenly distributed within the column and usually not located directly at the column wall. For a homogenous distribution profile, the liquid is uniformly distributed in all cells, including the wall cells. This results in a higher initial liquid wall flow than with a real distributor. Above the loading point, the increase of k_{wall} is relatively higher than the one for k_{bulk}. Therefore, the liquid wall flow fraction drops with rising gas loads. This is in good agreement with the experimental results in Figure 11 B.

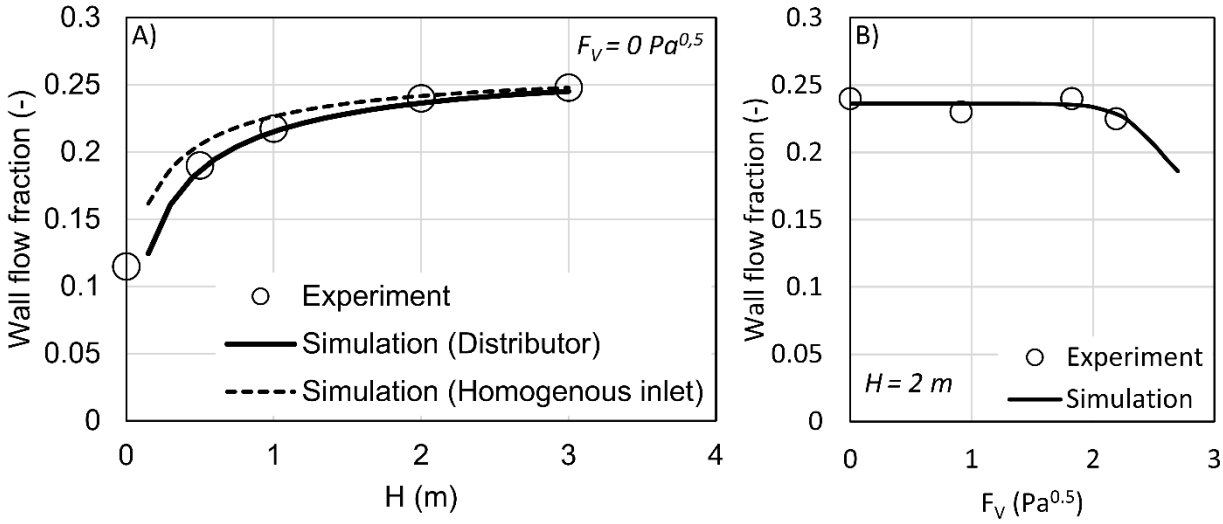

Figure 11: Comparison simulated and experimental wall flow by Kouri & Sohlo[33] in a scaled-up column of D = 0.5 m and u_L = 18 $m^3\ m^{-2}h^{-1}$

Figure 12 shows the validation of the simulated liquid distribution profiles at different column diameters, heights, and liquid inlet distributions. All profiles are in good agreement with the literature for a uniform liquid inlet distribution over the whole cross section of the column (Figure 12, A, C, D). In addition, the model is still in good agreement with literature data for a given initial maldistribution for a liquid inlet covering 64 % of the cross-sectional area in the center of the column (B). It can be concluded that the model can be successfully applied for scale-up, in addition to fluid dynamics and liquid distribution simulations. This provides the necessary basis for mass transfer simulations.

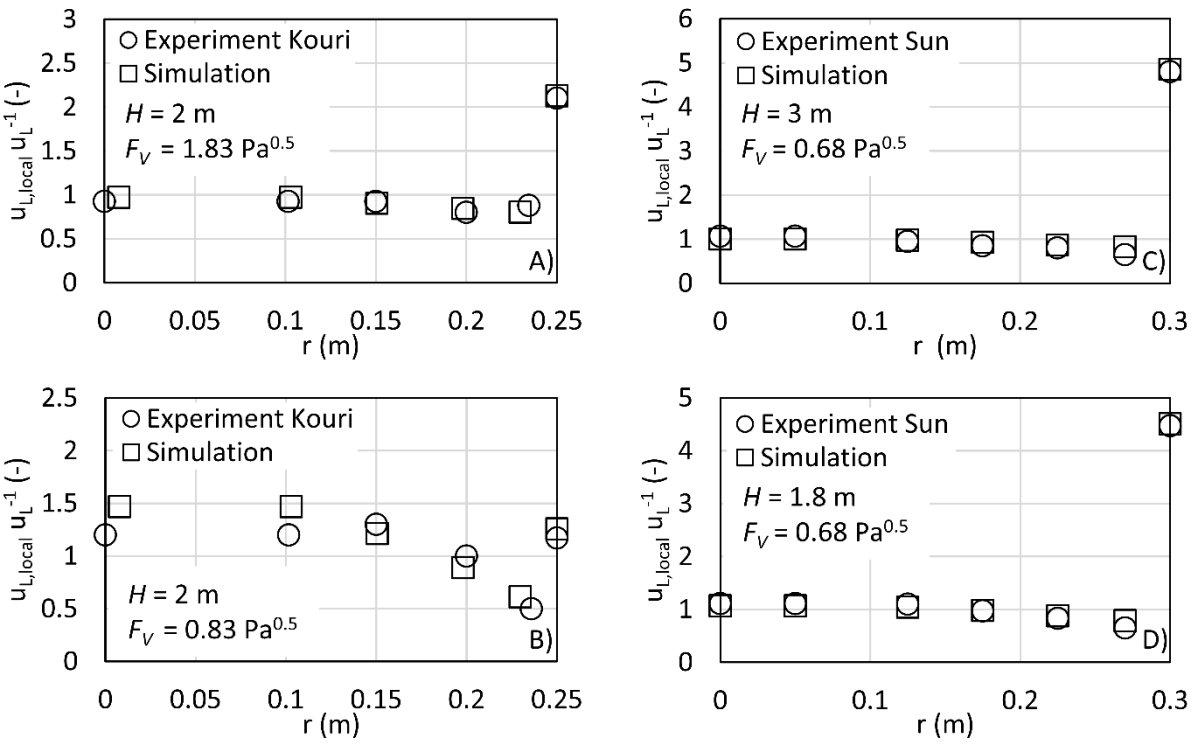

Figure 12: Simulated and experimental local flow profiles for A) complete cross-sectional liquid feed of u_L = 18 $m^3\ m^{-2}h^{-1}$ with a distributor (382 drip points)[33], B) homogenous liquid feed of u_L = 18 $m^3\ m^{-2}h^{-1}$ for 64 % of the column (centered liquid feed)[33], C) & D) homogenous liquid feed of u_L = 17 $m^3\ m^{-2}h^{-1}$ across the complete column cross section[46]

5.3 Mass transfer

Figure 13 A shows the influence of simulated maldistribution on HTU_{OL} compared to the predicted HTU_{OL} according to Billet & Schultes[35]. For u_L = 10 m^3 $m^{-2}h^{-1}$ the simulated HTU_{OL} are significantly higher, which indicates a lower mass transfer due to maldistribution. Moreover, the distance between the correlated HTU_{OL} at different liquid loads is larger than the simulated HTU_{OL}. This indicates that the loss of separation efficiency in the simulation is much less than predicted by the correlation. The reason for this behavior can be found by comparing wall and bulk flow. The maldistribution accounts for about 31 % of the total liquid flow at the packed bed height of H = 1.5 m. Thus, the liquid load in the bulk is lower than the average load, while there is a strong increase in liquid load close to the column wall.

According to literature[35], the liquid side limited HTU_{OL} is reduced with decreasing liquid load, which refers to a better overall mass transfer. This results from a reduced mass transfer coefficient due to lower liquid loads, but an increased residence time on the other hand. The same can be observed in the column bulk. The local liquid load decreases due to wall flow, while the overall mass transfer increases due to residence time. The opposite effect is observed in the wall region. While the local mass transfer coefficients are significantly higher due to the increased liquid load, the residence time decreases. Again, the residence time dominates the overall mass transfer and mass transfer at the column wall decreases strongly. With a higher overall mass transfer for the column bulk and a lower mass transfer at the column wall, the increase in HTU_{OL} with increasing liquid load predicted by the model is lower than the correlated one. It should be mentioned here that the HTU_{OL} of the Billet and Schultes correlation and the simulation are the same for plug flow without phase mixing and constant liquid and gas loads over the column cross section.

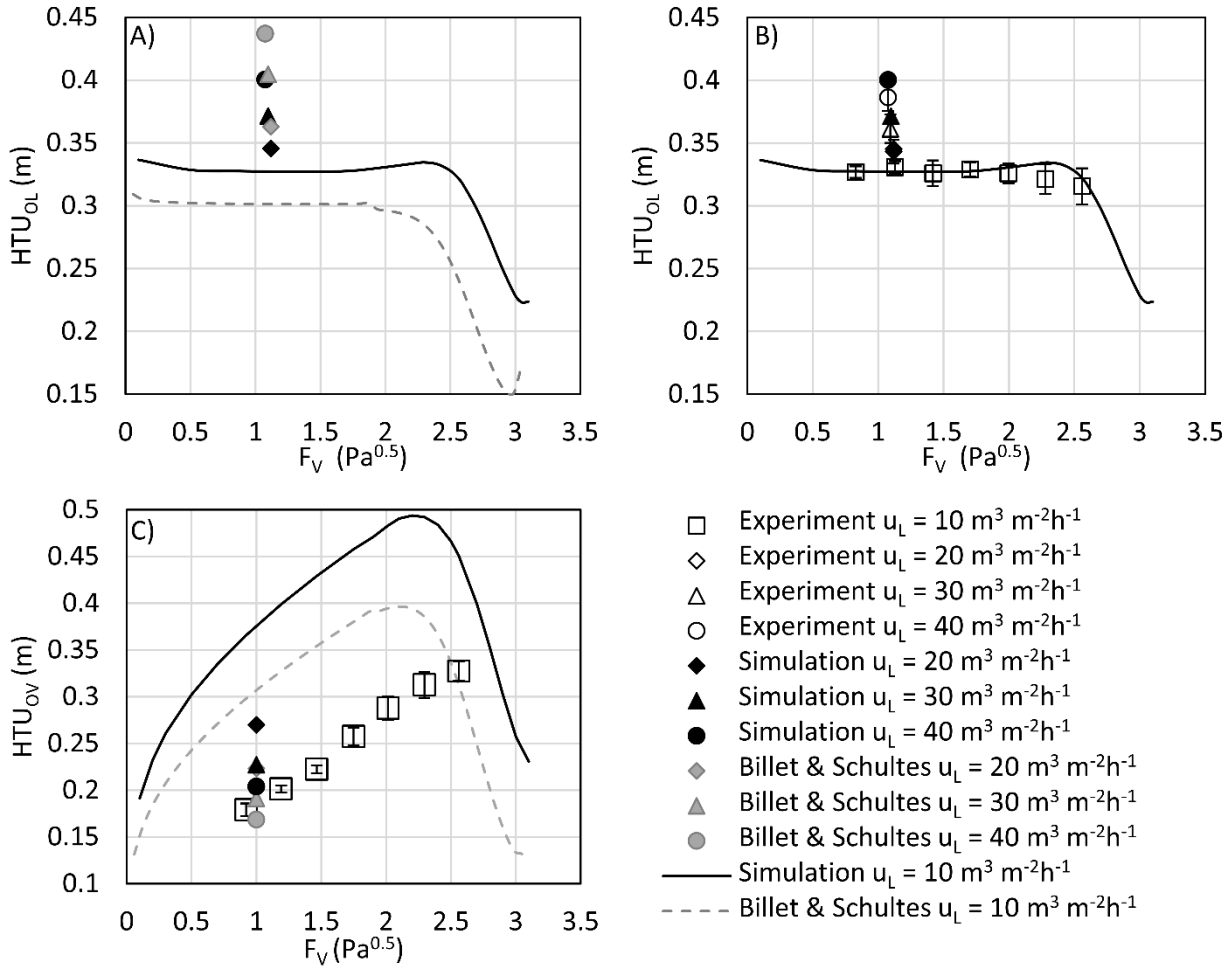

Figure 13: Comparison of liquid and gas side HTU between A) simulation and correlation for CO_2 desorption, B) simulation and experimental data for CO_2 desorption and C) simulation, correlation, and experiment for NH_3 absorption

These results are confirmed by the experimental data measured by CO_2 desorption for the Pall Ring 25 M, as presented in Figure 13 B. the simulated HTU_{OL} are in excellent agreement with the experimental. It can be concluded that the correlation of Billet and Schultes can be applied for local mass transfer coefficients within the model without further adjustments. On the other hand, the integral mass transfer parameters in Figure 13 A as predicted by the Billet and Schultes model do not agree well with the experimental results of this work in Figure 13 B, which could be subject of future investigations. The differences between experiment and correlation are most likely a result of different experimental conditions, which in this work are based on the standardized procedure according to the VDI 2761/2[7].

The overall gas side HTU_{OV} determined by NH_3 absorption are given in Figure 13 C. Again, the comparison of the simulation with the Billet and Schultes correlation shows the expected decrease in mass transfer due to maldistribution. In contrast to the liquid side mass transfer, the distance of steps for the gas side HTU_{OV} with increasing liquid load are almost constant for simulation and correlation. On the one hand, the decrease in liquid load in the bulk of the column induced by maldistribution reduces the effective phase interface and thus the gas-side mass transfer coefficients. On the other hand, the increase in mass transfer due to higher liquid loads at the column wall is less relevant due to the reduced residence time. Therefore, the influence of maldistribution on the overall gas side limited mass transfer is more pronounced than on the liquid side limited mass transfer.

For the HTU_{OV}, neither the Billet and Schultes model nor the simulations are in good agreement with the experimental results. This could also be attributed to some extent to the different standards for measurements today and in the past. However, Hoffmann et al.[47] also found large deviations between the correlation and own measurements with results that are close to the one obtained in this work. At this point, further clarification seems necessary. Nevertheless, the slopes of simulation, correlation and measurement below the loading point are in qualitatively good agreement. Above the loading point, the Billet and Schultes model predicts a strong increase in mass transfer, which was not observed in the experiments. Therefore, the Billet and Schultes model equations need an adjustment for the application as local correlations. In case of the Pall Ring 25 M, the local mass transfer coefficients would be increased by a factor of 3.45 to fit the experimental data below the loading point. This indicates, that especially for gas side mass transfer coefficient $\beta_G a_{eff}$, the correlation underestimates the local mass transfer that is present in the bulk of the laboratory or pilot column. Consequently, this would lead to an overdesign of an industrial size column.

6. Conclusion

Gas and liquid phase maldistribution are a problem not only for industrial sized columns, but also during the characterization of fluid dynamics and mass transfer coefficients, which are then used for

the design of industrial sized columns. A comprehensive model-based design and scale-up approach was developed that allows evaluation of the maldistribution effects on fluid dynamics and mass transfer at constant computational effort. For the first time, fluid distribution, gas distribution, fluid dynamics and rate-based mass transfer calculations were combined in a single model approach.

The presented cell model approach enables a local evaluation of fluid dynamics, mass transfer and phase distribution according to the chosen cell discretization. This work focuses on the description of the differences between wall and bulk cells. While fluid dynamics and rate-based mass transfer calculations are based on a common literature correlation, the liquid distribution parameters for wall and bulk are determined experimentally. The distribution parameters fitted to experimental data obtained by a wire-mesh sensor were proved to be independent of the liquid load and, below the loading point, of the gas load. The adaptation of the model parameters is not only limited to measurements with a wire-mesh sensor as used in this work, but can also be determined e.g., via spreading parameters and wall flows documented in the literature or experimental flow measurements. The gas distribution is modeled based on local pressure drop compensation in each cell layer. No solution of the momentum conservation equations is necessary.

The model-based column scale-up is possible by adapting the distribution coefficients to different column geometries, without increasing the cell number or discretization steps. Thus, computational effort for all column diameters and heights remains constant, allowing a calculation of different operating conditions and geometries within a few seconds, but on the cost of spatial resolution. However, the latter is often of secondary importance, especially in the case of a large-scale maldistribution. A general procedure for the adjustment of the distribution parameters to different column geometries is presented and was determined to be applicable for different column diameters and packed bed heights. The adaptability of the computing power thus enables easy integration of the model into flowsheeting programs, without influencing overall speed of the simulation significantly.

The model was found to be in excellent agreement with literature and experimental data for fluid dynamics and liquid distribution. Therefore, the model proved to be applicable to describe the influence of maldistribution on hold-up and pressure-drop calculations as well as local liquid loads. Based on this, investigations were carried out on the influence of maldistribution on mass transfer. Simulations showed the expected decrease of mass transfer due to maldistribution compared to the Billet and Schultes mass transfer correlation. Furthermore, the experimental HTU_{OL} agree well with the simulated ones, while the correlation neglects certain effects due to liquid maldistribution. Gas side mass transfer was found to be significantly lower compared to the experimental results. Therefore, further investigations are necessary with the aim to find new correlations for local mass transfer or modifications for current literature correlations to describe local mass transfer parameters, especially gas side parameters, with higher accuracy. Conversely, the presented model could be used to determine local mass transfer parameters based on experimental results or literature correlations by adjusting the packing-specific correlation constants in such a way that the simulations fit the experimental or correlated results.

Notation

A	m^2	Area
a	$m^2\ m^{-3}$	Specific packing surface
c	$mol\ m^{-3}$	Concentration
D_i	$m^2\ s^{-1}$	Diffusion coefficient
D	m	Column diameter
F_V	$Pa^{0,5}$	Gas capacity factor
$\dot{G}$	$m^3\ h^{-1}$	Gas flow
H	m	Packed bed height
H_G	$m^3\ m^{-3}$	Gas hold-up
H_L	$m^3\ m^{-3}$	Liquid hold-up
k	-	Distribution coefficient
$k_{OL}a$	$mol\ m^{-3}s^{-1}$	Overall liquid side mass transfer coefficient
M	$kg\ mol^{-1}$	Molar mass
m_{yx}	$mol\ m^{-3}\ (mol\ m^{-3})^{-1}$	Slope of the equilibrium line
$\dot{n}$	$mol\ h^{-1}$	Molar flow
Δp	Pa	Pressure drop
r	m	Radial coordinate
R	m	Radius
$signal$	-	Wire-mesh sensor signal
u_L	$m^3\ m^2h^{-1}$	Liquid load
$\bar{u}$	$m\ s^{-1}$	Mean film velocity
V	m^3	Volume
$\dot{V}$	$m^3\ h^{-1}$	Volume flow
x	$mol\ mol^{-1}$	Liquid molar fraction
y	$mol\ mol^{-1}$	Gas molar fraction
z	m	Axial packed bed position

Greek letters

β	m s^{-1}	Mass transfer coefficient
δ	m	Film thickness
η	Pa s	Dynamic viscosity
ρ	kg m^{-3}	Density

Subscripts

bulk	Column bulk
cell	Index for cell
down	Axial flow downward
eff	Effective interphase
Fl	Flooding point
flow	Cross sectional flow area
flux	Molar flux across the phase interface
G	Gas
gas	Gas distribution coefficient
i	Counting index
in	Flow into a cell or packing element
j	Area index for the j^{th} cell side area
L	Liquid
Layer	Index for cell-layer
local	Local liquid load
OG	Overall gas side
OL	Overall liquid side
out	Outflow from a cell or packing element
packing	Reference to the flow from one packing element
pot	Potential hold-up
S	Loading point
side	Lateral flow through a cell side
wall	Column wall

Abbreviations

HTU	Height of transfer unit
M	Metal
NTU	Number of transfer unit
P	Plastic

References

1. Billet R. Packed towers: In processing and environmental technology. Weinheim, New York: VCH, 1995.
2. Hoek PJ. Large and small scale liquid maldistribution in a packed column. PhD thesis. Delft University of Technology, 1983.
3. Albright MA. Packed tower distributors tested. Hydrocarb. Process. 1984;62(9):173–177.
4. Kister HZ. Distillation design. McGraw-Hill's AccessEngineering. New York: McGraw-Hill, 1992.
5. Maćkowiak J, Maćkowiak JF. Random Packings. In: Górak A, Olujic Z, editors. Distillation: Equipment and processes. London: Academic Press, 2014:85–144.
6. Schoenmakers H, Spiegel L. Laboratory Distillation and Scale-up. In: Górak A, Olujic Z, editors. Distillation: Equipment and processes. London: Academic Press, 2014:319–339.
7. Verein Deutscher Ingenieure. VDI 2761 Blatt 2: Thermische Trennverfahren in der Verfahrenstechnik: Messung und Auswertung von Fluiddynamik und Stofftransport in gepackten Kolonnen. Absorption und Desorption. Düsseldorf, 2018.
8. van Holt F. Optimierung und Erweiterung der Auslegung gepackter Kolonnen unter Berücksichtigung der Phasenverteilung. PhD thesis. Bochum: Ruhr-Universität-Bochum, 2020.

9. van Holt F, Hapke M, Grünewald M. Development of a Model Approach for the Phase Distribution in Packed Columns. Chem. Ing. Tech. 2019;91(1-2):102–109.
10. Grünewald M, Brinkmann J, Hapke M, van Holt F. Improved and Innovative Methods for the Characterization of Random and Structured Packings. Chem. Eng. Trans. 2018;69:103–108.
11. van Holt F, Grünewald M. Untersuchung der Phasendistribution in gepackten Kolonnen und Validierung eines Zellenmodells. Chem. Ing. Tech. 2019;91(4):435–443.
12. van Holt F, Brinkmann J, Grunewald M. Experimental and Theoretical Studies on Local Liquid Phase Distribution in Packed Columns. Chem. Eng. Trans. 2018;69:391–396.
13. Cihla Z, Schmidt O. A study of the flow of liquid when freely trickling over the packing in a cylindrical tower. Collect. Czech. Chem. C. 1957;22(3):896–907.
14. Amini Y, Nasr Esfahany M. CFD simulation of the structured packings: A review. Separation Science and Technology. 2019;54(15):2536–2554.
15. Jameson GJ. A model for liquid distribution in packed columns and trickle-bed reactors. Trans. Inst. Chem. Eng. 1966;44:T198-T206.
16. Baker T, Chilton TH, Vernon HC. The course of liquor flow in packed towers. Trans. AIChE. 1935;31:296–315.
17. Herskowitz M, Smith JM. Liquid distribution in trickle-bed reactors: Part I. Flow measurements. AIChE J. 1978;24(3):439–450.
18. Herskowitz M, Smith JM. Liquid distribution in trickle-bed reactors: Part II. Tracer studies. AIChE J. 1978;24(3):450–454.
19. Stikkelman RM. Gas and liquid maldistributions in packed columns. TU Delft: PhD Thesis, 1989.

20. Wen X, Shu Y, Nandakumar K, Chuang KT. Predicting liquid flow profile in randomly packed beds from computer simulation. AIChE J. 2001;47(8):1770–1779.
21. Nandakumar K, Shu Y, Chuang KT. Predicting geometrical properties of random packed beds from computer simulation. AIChE J. 1999;45(11):2286–2297.
22. Wild A, Engel V. Ein neuartiges Zellenmodell zur Maldistributions und Verteilgütenbestimmung. Processnet Fachgruppe Fluidverfahrenstechnik. Karlsruhe, 2007.
23. Wild A, Engel V, Hanusch F, Rehfeldt S, Klein H. Zellenmodell zur Auslegung von Packungskolonnen Teil 2: Das WelChem–Zellenmodell zur Berechnung der Maldistribution. Chem. Ing. Tech. 2015;87.
24. Hanusch F, Rehfeldt S, Klein H. Zellenmodell zur Auslegung von Packungskolonnen Teil 1: Untersuchung der Flüssigkeitsverteilung in Füllkörperpackungen. Chem. Ing. Tech. 2015;87.
25. Hanusch F, Kender R, Engel V, Rehfeldt S, Klein H. TUM–WelChem cell model for the prediction of liquid distribution in random packed columns. AIChE J. 2019;89(11):e16598.
26. Zuiderweg FJ, Hoek PJ, Lahm Jj. The effect of liquid distribution and redistribution on the separating efficiency of packed columns: Einfluss der Fluessigkeitsverteilung und -umverteilung auf die Trennleistung von Fuellkoerperkolonnen. Inst. Chem. Eng. Symp. Series. 1987;(104):217–231.
27. Zuiderweg FJ, Kunesh JG, King DW. A Model for the Calculation of the Effect of Maldistribution on the Efficiency of a Packed Column. Chem. Eng. Res. Des. 1993;71(1):38–44.

28. Song M, Yin FH, Chuang KT, Nandakumar K. A stochastic model for the simulation of the natural flow in random packed columns. Can. J. Chem. Eng. 1998;76(2):183–189.
29. Higler A, Krishna R, Taylor R. Nonequilibrium Cell Model for Packed Distillation Columns - The Influence of Maldistribution. Ind. Eng. Chem. Res. 1999;38(10):3988–3999.
30. Potthoff R. Maldistribution in Füllkörperkolonnen. Fortschritt-Berichte VDI Reihe 3. Vol. 294. Düsseldorf: VDI-Verlag, 1992.
31. Schneider O. Maldistribution in Packungskolonnen: Ausmaß, Auswirkungen und Gegenmaßnahmen. Fortschritt-Berichte VDI Reihe 3, Verfahrenstechnik. 823/3. Düsseldorf: VDI-Verlag, 2004.
32. Kammermaier F. Neuartige Einbauten zur Unterdrückung der Maldistribution in Packungskolonnen. PhD thesis. Technische Universität München, 2008.
33. Kouri RJ, Sohlo J. Liquid and gas flow patterns in random packings. Chem. Eng. J. Bioch. Eng. 1996;61(2):95–105.
34. Duss M. A new method to predict the susceptibility to form maldistribution in packed columns based on pressure drop correlations. Inst. Chem. Eng. Symp. Series. 2006; (152):418–430.
35. Billet R, Schultes M. Prediction of Mass Transfer Columns with Dumped and Arranged Packings. Chem. Eng. Res. Des. 1999;77(6):498–504.
36. Kraume M. Transportvorgange in der Verfahrenstechnik: Grundlagen Und Apparative Umsetzungen. Springer Verlag, 2012.
37. Maćkowiak J. Fluid Dynamics of Packed Columns: Principles of the Fluid Dynamic Design of Columns for Gas/Liquid and Liquid/Liquid Systems. Chemical engineering. Heidelberg: Springer, 2010.

38. Dzhonova-Atanasova D, Kolev N, Nakov S. Determination of Liquid Radial Spreading Coefficients of Some Highly Effective Packings. Chem. Eng. Technol. 2007;30(2):202–207.
39. Fourati M, Roig V, Raynal L. Liquid dispersion in packed columns: Experiments and numerical modeling. Chem. Eng. Sci. 2013;100:266–278.
40. Staněk V, Kolář V. Distribution of liquid over a random packing. III. Distribution of liquid in a low bed of packing wetted by a thin stream of liquid; Determination of the coefficient of radial spreading of liquid. Collect. Czech. Chem. C. 1968;33(4):1049–1061.
41. Verein Deutscher Ingenieure, VDI-Gesellschaft Verfahrenstechnik und Chemieingenieurwesen. VDI-Wärmeatlas: Mit 320 Tabellen (11th edition). VDI-Buch. Berlin: Springer Vieweg, 2013.
42. Pohorecki R, Moniuk W. Kinetics of reaction between carbon dioxide and hydroxyl ions in aqueous electrolyte solutions. Chem. Eng. Sci. 1988;43(7):1677–1684.
43. Weigand B, Köhler J, Wolfersdorf Jv. Thermodynamik kompakt (3rd edition). Springer-Lehrbuch. Berlin, Heidelberg: Springer Vieweg, 2013.
44. Wilke CR, Lee CY. Estimation of Diffusion Coefficients for Gases and Vapors. Ind. Eng. Chem. 1955;47(6):1253–1257.
45. Sander R. Compilation of Henry's law constants (version 4.0) for water as solvent. Atmos. Chem. Phys. 2015;15(8):4399–4981.
46. Sun CG, Yin FH, Afacan A, Nandakumar K, Chuang KT. Modelling and Simulation of Flow Maldistribution in Random Packed Columns with Gas-Liquid Countercurrent Flow. Chem. Eng. Res. Des. 2000;78(3):378–388.
47. Hoffmann A, Maćkowiak JF, Górak A, Haas M, Löning J-M, Runowski T, Hallenberger K. Standardization of Mass Transfer Measurements: A Basis for the Description of Absorption Processes. Chem. Eng. Res. Des. 2007;85(1):40–49.